Improving Dynamics of an Aerial Manipulator with Elastic Suspension Using Nonlinear Model Predictive Control

Arda Yigit, Miguel Arpa Perozo, Loic Cuvillon, Sylvain Durand, Jacques Gangloff

Improving Dynamics of an Aerial Manipulator with Elastic Suspension Using Nonlinear Model Predictive Control

Arda Yiğit, Miguel Arpa Perozo, Loïc Cuvillon, Sylvain Durand and Jacques Gangloff

***Abstract*— Aerial manipulation increases significantly the workspace size of robotic manipulators. However, aerial manipulation suffers from a lack of autonomy due to limited embedded energy. The Aerial Manipulator with Elastic Suspension (AMES) is designed to cope with this issue. It is an omnidirectional aerial vehicle equipped with a gripper and suspended under a robotic carrier by a spring for gravity compensation. In this paper, the AMES is controlled with a nonlinear model predictive controller (NMPC). To eliminate the steady-state errors, an observer based on a model of the AMES augmented with constant disturbances is implemented in conjunction with the NMPC controller. Experiments illustrate the efficiency of the NMPC by comparing it to a computed torque controller.**

I. INTRODUCTION

Aerial manipulation increases significantly the workspace size of robotic manipulators. Most common configurations for such robots are flying hands, where a gripper is attached to an unmanned aerial vehicle (UAV), and unmanned aerial manipulators, where one or more robotic arms are carried by a UAV [1].

Omnidirectional aerial vehicles can generate a six-degrees-of-freedom (6-DoF) wrench and so are suitable for manipulation tasks without need for an embedded robotic arm. These vehicles can use either fixed or orientable propellers. While six bidirectional (whose thrust can be reversed) fixed actuators are enough to control all DoFs, a redundant design with at least seven actuators is needed when using unidirectional propellers [2].

Brescianini and D'Andrea developed an omnidirectional multirotor vehicle actuated by eight nonparallel bidirectional thrusters. They are positioned in an optimal configuration maximizing the agility, i.e. the highest thrust and torque that can be generated on all directions, while enforcing rotational invariance [3]. The position and the attitude control loops are decoupled. Nonlinearities are canceled with a feedback linearization approach. A control allocation computes the rotor velocity input signal by minimizing the power consumption while limiting the difference between the desired thrust and the actual thrust. An external tachometer is used to regulate the rotor rotational velocity.

The ODAR is another aerial vehicle, designed for omnidirectional aerial wrench generation [4]. The eight nonparallel bidirectional thrusters are positioned to maximize the minimum-guaranteed omnidirectional wrench. A control allocation technique using a selective mapping algorithm is proposed to avoid the destabilizing effect of sensorless electronic speed controllers (ESCs) at low speeds.

The OMAV uses 6 pairs of orientable coaxial propellers for actuation [5]. A nonlinear model predictive controller (NMPC) computes the desired wrench. An allocation problem is then solved at a higher frequency to translate the wrench into actuator control signals. The NMPC handles constraints on the dynamic model of the system, limiting the maximum wrench and its rate of change. The plant model is augmented with constant disturbances corresponding to unmodeled dynamics. An extended Kalman filter (EKF) observes these disturbances, allowing for zero steady-state error. The controller is implemented on an onboard computer with the ACADO framework [6].

Bicego et al. used a more accurate actuator-level model for the NMPC [7]. Therefore, they took into account actuator dynamics and imposed more meaningful constraints on the propeller speed and acceleration. With this approach, the allocation problem is included into the NMPC optimization problem. Thereby, it is suitable for a large range of aerial robots, from under-actuated to fully-actuated platforms. Moreover, this strategy is compatible with both bidirectional and unidirectional actuators, since the NMPC can handle those constraints. The controller is implemented on a distant computer with the MATMPC framework [8] using the qpOASES solver.

Aerial manipulators suffer from low autonomy, due to the low energy density of lithium batteries. Tethering the aerial vehicle could provide unlimited autonomy by powering through the cable [9]. Furthermore, the suspension of the aerial vehicle reduces energy consumption thanks to gravity compensation. The cable-suspended aerial manipulator SAM [10], [11] is an omnidirectional aerial manipulator suspended by winch-actuated cables under an aerial carrier that carries a 7-DoF serial manipulator. The aerial carrier is supposed to be static. The SAM regulates its pose with a cascade proportional-derivative control scheme.

Recently, we introduced an aerial manipulator with elastic suspension (AMES). Instead of the cable+winch subsystem of the SAM, we propose to use a low-stiffness spring [12]. The spring decouples the aerial vehicle from its carrier, so its motion is not limited anymore by the dynamics of the winches. A computed torque control law was proposed and its stability was proven assuming instantaneous allocation of the control inputs and the absence of actuator saturations.

In this work, we upgrade the computed torque controller

This work was supported by the e-VISER project under grant ANR-17-CE33-0008 by the French National Research Agency (ANR).

The authors are with the ICube Laboratory, University of Strasbourg, INSA Strasbourg, 67000, Strasbourg, France. E-mails: {arda.yigit, marpaperozo, l.cuvillon, sdurand, jacques.gangloff}@unistra.fr

(CTC) of the AMES by replacing it with a NMPC. Thus, a more accurate model of the AMES including actuator dynamics and saturations can be considered, allowing improved dynamic performance. A constant disturbance model and an EKF-based observer are used to achieve a zero steady-state error. The NMPC is implemented using acados [13], a state-of-the-art code generation tool for optimal control problems, and HPIPM [14], an efficient QP solver for small to medium sized problem. We illustrate the efficiency of the NMPC by comparing its experimental performance with respect to the CTC.

II. Robot description

Inspired by our previous works [15], [16], where additional embedded thrusters were used to improve the dynamics of cable-driven parallel robots, we developed a novel aerial manipulator with elastic suspension [12] shown in Fig. 1. The aerial manipulator is suspended at the tip of a crane-like robotic carrier by a spring. The aerial manipulator, which is called here an Aerial Wrench Generator (AWG), is holding a gripper. The purpose of the AWG is to generate a 6-DoF wrench at the end effector of the AMES thanks to its propulsion units. So the AMES with its robotic carrier, spring and AWG may be considered as a hybrid between a serial manipulator and an aerial manipulator with a spring acting as a flexible linkage.

The low-stiffness spring compensates for the gravity, so the AWG is almost free-floating in the air around its equilibrium position, and therefore, unlike a UAV, requires little energy. Moreover, there is no more need to use an actuated winch to control the altitude.

The robotic carrier is optional. It aims to move slowly the equilibrium position of the AWG to the average position of the current task, reducing the energy consumption, and increasing the workspace even more.

III. Modeling

The dynamics of the robotic carrier are supposed to be slower than the AWG dynamics. Thereby, the anchoring point of the spring is considered static during this study. Besides, the mass of the load is assumed to be negligible.

A. System parameters and notations

The geometric parameters of the system are displayed in Fig. 2. The following model makes no assumptions on the number of propulsion units (can be under- or over-actuated), nor on their directionality (unidirectional or bidirectional).

The origin O of the inertial frame $\mathcal{R}_f = (O, \mathbf{x^f}, \mathbf{y^f}, \mathbf{z^f})$ is the static anchoring point of the spring, while A is its mobile end. The body frame $\mathcal{R}_b = (G, \mathbf{x^b}, \mathbf{y^b}, \mathbf{z^b})$ is positioned at the center of mass (CoM) G of the AWG, its $\mathbf{z^b}$ axis points toward A. The rotation matrix $\mathbf{R_{fb}} \in SO(3)$ describes the orientation of $\mathcal{R}_b$ with respect to $\mathcal{R}_f$. The AWG has n propulsion units, positioned in an arbitrary way. The position of the center of the i-th propulsion unit is B_i, and $\mathbf{u^i}$ is the thrust direction. The position vector of the CoM G is $\mathbf{p}$.

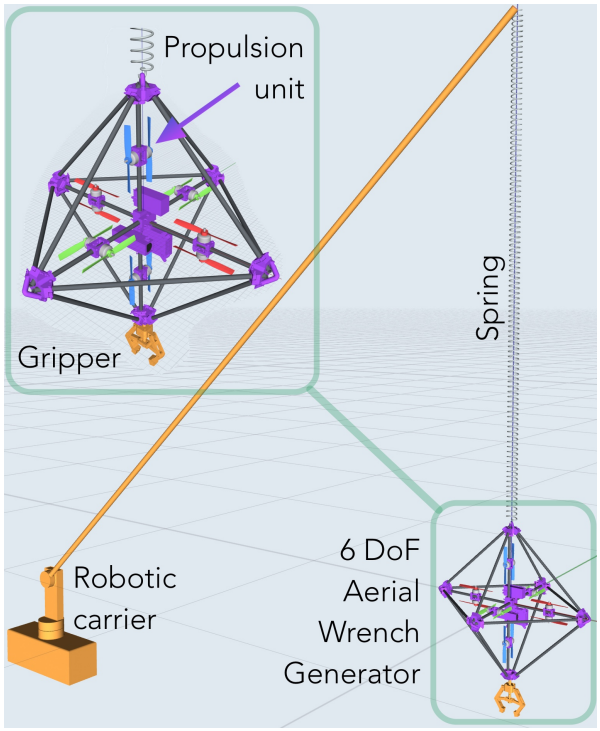

Fig. 1. AMES concept.

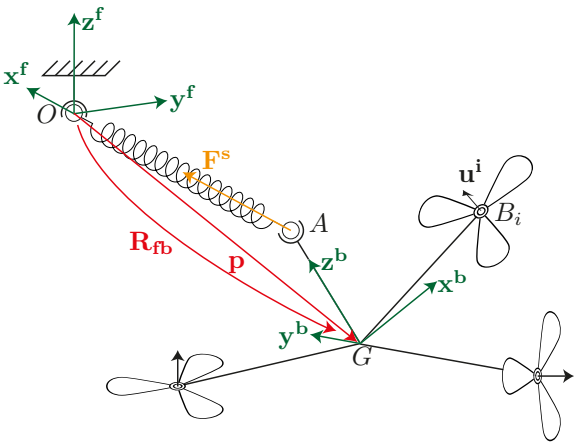

Fig. 2. Geometric parametrization of the i-th propulsion unit.

Let $\boldsymbol{\alpha}$ and $\boldsymbol{\beta}$ be vectors and $\mathcal{R}_q$ a reference frame. The projection of $\boldsymbol{\alpha}$ in $\mathcal{R}_q$ is written $\boldsymbol{\alpha}_q$. The cross product of $\boldsymbol{\alpha}_q$ and $\boldsymbol{\beta}_q$ is denoted $\boldsymbol{\alpha}_q \times \boldsymbol{\beta}_q$ and $[\cdot]_\times$ is the cross product matrix such that $\boldsymbol{\alpha}_q \times \boldsymbol{\beta}_q = [\boldsymbol{\alpha}_q]_\times \boldsymbol{\beta}_q$.

B. AWG dynamics

The inertia of the rotating parts is assumed negligible, dismissing the gyroscopic effect and the acceleration torque. Besides, the spring is considered massless. Thereby, the AWG can be modeled as a single body and its dynamics derived using Euler's laws of motion:

$$m\ddot{\mathbf{p}}_f - m\mathbf{g}_f - \mathbf{F}^{\mathbf{s}}_f = \mathbf{F}_f \tag{1}$$

$$\mathbf{J}_b\dot{\boldsymbol{\omega}}_b + \boldsymbol{\omega}_b \times \mathbf{J}_b\boldsymbol{\omega}_b - \mathbf{N}^{\mathbf{s}}_b = \mathbf{N}_b \tag{2}$$

where m is the mass of the AWG, $\mathbf{g}$ the gravity acceleration vector, $\mathbf{J}_b$ the inertia tensor at the center of gravity expressed in the body frame $\mathcal{R}_b$, $\boldsymbol{\omega}$ the angular velocity vector of the AWG with respect to the inertial frame $\mathcal{R}_f$, $\mathbf{F^s}$ the force exerted by the spring on the AWG and $\mathbf{N^s}$ the associated torque at the center of mass, $\mathbf{F}$ and $\mathbf{N}$ the force and torque developed by the propellers at the center of mass.

Let $\boldsymbol{\eta} = (\psi\ \theta\ \phi)^T$ be a set of Euler angles describing the orientation of the body frame $\mathcal{R}_b$ with respect to the inertial frame $\mathcal{R}_f$. The analytical Jacobian matrix $\mathbf{S}(\boldsymbol{\eta})$ maps the time derivative of $\boldsymbol{\eta}$ to the angular velocity $\boldsymbol{\omega}_b$:

$$\boldsymbol{\omega}_b = \mathbf{S}(\boldsymbol{\eta})\dot{\boldsymbol{\eta}} \tag{3}$$

The force generated by the spring on the AWG depends on its stiffness k and free length l_0:

$$\mathbf{F}_f^{\mathbf{s}} = -k\left(\|\mathbf{OA}\| - l_0\right)\frac{\mathbf{OA}_f}{\|\mathbf{OA}\|}$$

where

$$\mathbf{OA}_f = \mathbf{p}_f + \|\mathbf{GA}\|\,\mathbf{R_{fb}}\mathbf{z_b^b}$$

Therefore, the associated torque is as follows:

$$\mathbf{N}_b^{\mathbf{s}} = \|\mathbf{GA}\|\,\mathbf{z}_b^{\mathbf{b}} \times \mathbf{R}_{\mathbf{fb}}^T\mathbf{F}_f^{\mathbf{s}}$$

The thrust and the drag generated by a propeller are proportional to the squared rotational speed of the propeller and oriented along the propeller axis [17]. Let a be the thrust coefficient, b the drag coefficient and $\mathbf{W}_b \in \mathbb{R}^{6\times n}$ the matrix that maps the signed squared propeller rotational velocities $\mathbf{w}_2 = (\cdots\ w_i|w_i|\ \cdots)^T$ to the wrench the propulsion units apply on the platform:

$$\begin{pmatrix}\mathbf{F}_b\\ \mathbf{N}_b\end{pmatrix} = \mathbf{W}_b\mathbf{w}_2 \tag{4}$$

$$\mathbf{W}_b = a\begin{pmatrix}\cdots & \mathbf{u_b^i} & \cdots\\ \cdots & \mathbf{GB_b^i}\times\mathbf{u_b^i} & \cdots\end{pmatrix} + b\begin{pmatrix}\cdots & \mathbf{0}_{3\times1} & \cdots\\ \cdots & \mathbf{u_b^i} & \cdots\end{pmatrix}$$

We suppose that the rotational velocity of all propellers is regulated with independent low-level control loops. The actuator dynamics relate the actual rotational velocity w_i of a propeller with respect to the reference w_i^* of the velocity control loop, with $i \in [\![1, n]\!]$. They are modeled as a first-order dynamic system of time constant t_m:

$$t_m\dot{\mathbf{w}} = \mathbf{w}^* - \mathbf{w} \tag{5}$$

with $\mathbf{w} = (\dots\ w_i\ \dots)^T$ and $\mathbf{w}^* = (\dots\ w_i^*\ \dots)^T$.

IV. NONLINEAR MODEL PREDICTIVE CONTROL

A. Problem formulation

Let $\mathbf{x}$ be the vector of continuous state variables for the plant model:

$$\mathbf{x} = \left(\mathbf{p}_f^T\ \boldsymbol{\eta}^T\ \dot{\mathbf{p}}_f^T\ \boldsymbol{\omega}_b^T\ \mathbf{w}^{*T}\ \mathbf{w}^T\right)^T$$

and $\mathbf{u} = \dot{\mathbf{w}}^*$ the control input of the system. The time derivative of the propeller velocity reference is selected as control input, such that this input is zero in steady state. That property is desirable for the optimal control problem (OCP) formulation introduced below to be well conditioned. The AWG dynamics (1), (2), (3) with its actuator model (5) can be described by a set of differential equations:

$$\dot{\mathbf{x}} = \mathbf{f}(\mathbf{x}, \mathbf{u}) \tag{6}$$

A NMPC is proposed to track a 6-DoF reference trajectory based on this model of the AWG. The optimal control problem consists in minimizing a quadratic objective function under constraints of the nonlinear plant model and state or input saturations:

$$\begin{aligned}\min_{\mathbf{u},\mathbf{x}}\ & \left[\int_0^T \left(\|\mathbf{y}(t) - \mathbf{y^r}(t)\|_{\mathbf{Q}}^2 + \|\mathbf{u}(t)\|_{\mathbf{R}}^2\right)dt\right]\\ \text{subject to}\ & \dot{\mathbf{x}} = \mathbf{f}(\mathbf{x}, \mathbf{u})\\ & \mathbf{x}(0) = \mathbf{x_0}\\ & \mathbf{h}(\mathbf{x}, \mathbf{u}) \geq \mathbf{0}\end{aligned} \tag{7}$$

where $\mathbf{y} = (\mathbf{p}^T\ \boldsymbol{\eta}^T\ \dot{\mathbf{p}}^T\ \boldsymbol{\omega}_b^T)^T \subset \mathbf{x}$ is the controlled state variable, $\mathbf{y^r}$ the reference, $\mathbf{x_0}$ the initial state, $\mathbf{h}(\mathbf{x}, \mathbf{u}) \geq \mathbf{0}$ a set of constraints and T the prediction horizon length. The operator $\|\cdot\|_{\mathbf{P}}$ is defined such that $\|\mathbf{v}\|_{\mathbf{P}}^2 = \mathbf{v}^T\mathbf{P}\mathbf{v}$. The weighting matrices $\mathbf{Q}$ and $\mathbf{R}$ are positive definite. The controller is tuned by adjusting the weights of the controlled variables in the OCP through these matrices.

B. Disturbance observer design

External disturbance, such as wind, and unmodelled or inaccurate dynamics can cause a steady-state error on the AWG pose. Indeed, there is no guarantee that the optimal control input will enforce a zero steady-state error if the OCP problem is solved based on an inaccurate model of the plant dynamics.

At steady state, i.e. $\dot{\mathbf{x}} = 0$, we assume that there are no external disturbance and no error on the propeller velocity due to the integral action of an inner control loop. Therefore, the only source of errors is due to the inaccurate dynamics model of the AWG.

To estimate these modeling errors, an EKF implements the plant model augmented with constant disturbances:

$$\underbrace{\begin{pmatrix}\dot{\mathbf{x}}\\ \dot{\mathbf{d}}\end{pmatrix}}_{\dot{\mathbf{x}}_\mathbf{a}} = \underbrace{\begin{pmatrix}\mathbf{f}(\mathbf{x}, \mathbf{u}) + \mathbf{B_d}\mathbf{d}\\ \mathbf{0}\end{pmatrix}}_{\mathbf{f_a}(\mathbf{x_a}, \mathbf{u})} \tag{8}$$

where $\mathbf{d}$ is a vector of six disturbance variables to take into account the AWG modeling errors and $\mathbf{B_d} = (\mathbf{0}_{6\times6}\ \mathbb{I}_{6\times6}\ \mathbf{0}_{6\times12})^T$ is a matrix that maps disturbances to the derivatives of $\dot{\mathbf{p}}$ and $\boldsymbol{\omega}_b$.

These estimated disturbances are fed back to the NMPC (see Fig. 3) which will reject them based on the augmented model resulting in a zero steady-state error.

Note that as the number of added disturbances is lower that the number of controlled variables, the above method does not ensure offset-free errors for other disturbances that the AWG dynamics [18]. However, by limiting the number of added disturbances, the size of the augmented system and, thereby, the OCP computation burden are reduced.

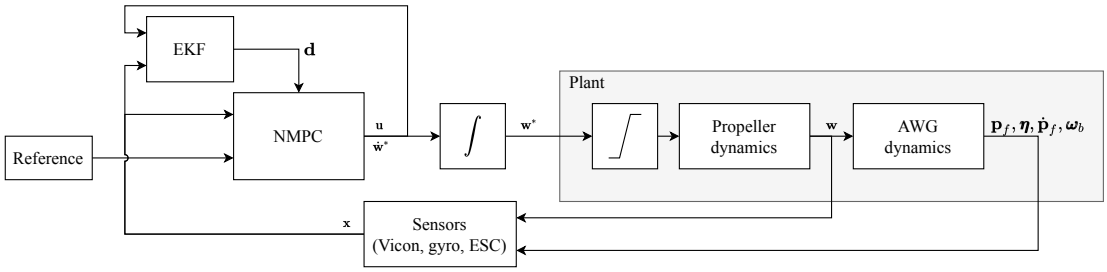

Fig. 3. Block diagram.

V. EXPERIMENTAL SETUP

A. Mechanical design

The AWG has the same structure as an omnidirectional multirotor vehicle with bidirectional thrusters described in [3] with $n = 6$ propulsion units. This configuration can generate a 6-DoF wrench without over-actuation, simplifying the thrust allocation problem. With this configuration, the propulsion units are attached to the vertices of a regular octahedron.

Depending on its mass, the transverse vibrations of the spring can significantly disturb the AWG. That can be avoided by mounting the spring horizontally and suspending the AWG by a cable through a pulley (see Fig. 4).

Some ESCs can drive a motor in both directions. Combined with symmetrical propellers (also called 3D propellers), one can use them to generate force in both directions. However, as shown in [4], if a change of rotation direction occurs, i.e. if the velocity crosses zero, the settling time is longer than the settling time without direction change. Indeed, ESCs use the back EMF (electromotive force) to estimate the speed of the rotor, which is not possible at low speeds. For a standard multirotor drone, this may not be a real issue since propellers need to generate a high force continuously in order to hover, but it is a limiting factor for the AMES, where propellers may need to change the rotation direction many times per second (for example, the natural frequency for roll/pitch angles of the robot is higher than $3\,\mathrm{Hz}$).

Each propulsion unit (Fig. 4) is made of a pair of propellers (DALPROP 5045), mounted on two coaxial brushless DC motors (T-Motor F-40 Pro III Kv2400), in order to be able to generate a force in both directions without changing direction of rotation, avoiding the "zero-crossing" problem. According to the sign of the force to be generated, the corresponding propeller rotates at the desired speed while the second one is idling, i.e. rotating at its lowest speed ($1500\,\mathrm{rpm}$, equivalent to $0.03\,\mathrm{N}$).

B. Electronics

Each propeller is driven by a brushless DC motor. There is only a limited number of commercial ESCs providing speed regulation and most of them are designed for helicopters and do not have fast dynamics. We use the open-source Teensyshot firmware developed in our lab (https://github.com/jacqu/teensyshot) for the high bandwidth digital speed control of brushless DC motors without additional sensors. KISS 32A ESCs are used for the experiments.

The AWG is autonomous, it carries its own energy source: a $2300\,\mathrm{mA\,h}$, 3S lithium polymer battery pack (TATTU 3S1P). It also has an on-board CPU (Raspberry Pi 4B) running high-level control algorithms and communicating with a ground station through Wi-Fi TCP/IP sockets thanks to the open-source Simulink toolbox RPIt developed in our lab [19]. The Raspberry Pi is connected by USB to 2 Teensy boards regulating the velocity of a total of 12 propellers.

The pose and the twist of the AWG are acquired by a Vicon Bonita motion-capture system (see Fig. 4) measuring the 6-DoF pose vector of the AWG with a refresh rate of $240\,\mathrm{Hz}$ and a gyroscopic sensor (MPU-9150).

C. Controller implementation/software architecture

The NMPC is implemented using acados [13], a recent open-source framework that generates efficient low-level code for optimization-based control. The continuous OCP (7) is discretized with a multiple shooting method and then solved with the HPIPM solver [14]. For real-time compliance, acados performs the Real-Time Iteration scheme that enables a reasonably fast computation of the NMPC output, but at the cost of a sub-optimal solution [20].

For compatibility issues of acados on 32-bit architectures, the controller runs on a distant computer equipped with an Intel i5-9500 processor. The distant computer hosts a TCP/IP server. The server receives the input data of the controller (setpoint and estimated state) from the embedded computer, and sends back the control input and the estimated next state.

D. Controller tuning

The propeller speed control loop is tuned such that, in closed loop, it behaves like a first-order system with $25\,\mathrm{ms}$ time constant. This model does not hold at high speeds due to current limitations. Hence, the propeller speed is limited to $22\,000\,\mathrm{rpm}$ by adding a constraint on the corresponding state in the OCP. The rate of change of the desired propeller speed can also be bounded to include motor current saturations [7].

The NMPC runs at $100\,\mathrm{Hz}$ with a $0.5\,\mathrm{s}$ prediction horizon. To track a reference trajectory, we control the pose and the twist of the AWG:

$$\mathbf{y} = \left(\mathbf{p}^T\ \boldsymbol{\eta}^T\ \mathbf{v}^T\ \boldsymbol{\omega}^T\right)^T$$

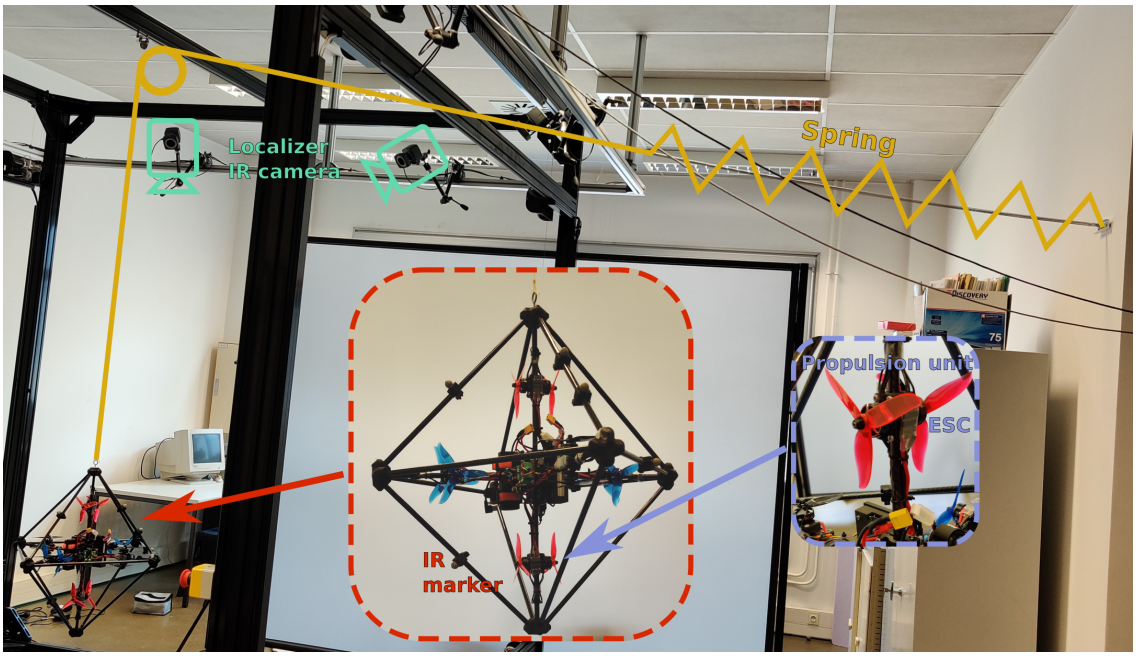

Fig. 4. Experimental setup with dextAIR v2 prototype.

The weighting matrices $\mathbf{Q}$ and $\mathbf{R}$ are diagonal:

$$\mathbf{Q} = diag(\mathbf{Q_p}, \mathbf{Q_\eta}, \mathbf{Q_v}, \mathbf{Q_\omega})$$

$$\mathbf{R} = R_u \mathbf{I}_{n\times n}$$

The weight values given in Table I were tuned using a trial-and-error procedure. In particular, the weight associated to the control input is significantly smaller by several orders of magnitude than the other weights because of its wide range of variation. Indeed, according to the first-order model assumption for the actuators, the propeller speed can approach its saturation value in less than $100\,\mathrm{ms}$. The control input, which is the rate of change of the propeller speed, can therefore exceed $10\,000\,\mathrm{rad\,s^{-1}}$ (and its square $10^8\,\mathrm{rad^2\,s^{-2}}$).

TABLE I
NMPC TUNING PARAMETERS.

Parameter	Diagonal entries	Parameter	Diagonal entries
$\mathbf{Q_p}$	$150, 150, 150$	$\mathbf{Q_\omega}$	$0.1, 0.1, 0.02$
$\mathbf{Q_\eta}$	$10, 10, 5$	R_u	$1.25e-10$
$\mathbf{Q_v}$	$0.02, 0.02, 0.02$		

VI. EXPERIMENTAL RESULTS

In this section, a set of experimental results are presented to assess the performances of the NMPC. The performance of a CTC with an integral action is used for comparison.

Roll, pitch and yaw angles are used to describe the orientation of the AWG. In the following experiments, these angles stay small, and therefore, far from singular configurations.

A. Step response

The step responses and the control inputs of the propulsion units in Fig. 5 compare the NMPC and the CTC for a large step reference along the x axis. The NMPC yields dynamics comparable to the CTC, but with significantly less overshoot. Indeed, with actuation saturation, a significant position error is accumulated in the integral term of the CTC during the travel to the setpoint. It results in an integral windup yielding an excessive overshoot while the accumulated error is dissipating. On the other hand, the NMPC anticipates the new reference and actuation saturation, enabling smooth variations of the control inputs. Furthermore, the noise sensitivity of the NMPC is reduced, as seen on the input control signals on lower plots of Fig. 5.

The rise times and the overshoots are summarized in Table II for $0.12\,\mathrm{m}$ step references along the x, y and z axes.

TABLE II
STEP RESPONSES

Axis	x	y	z
Rise time [s] CTC	0.13	0.13	0.14
Rise time [s] NMPC	0.18	0.18	0.19
Overshoot [%] CTC	95.7	110.6	71.1
Overshoot [%] NMPC	14.0	19.0	9.9

B. Trajectory tracking

To assess the trajectory tracking performance, the AWG is following the square-shaped trajectory in Fig. 6 using a trapezoidal velocity profile. The NMPC allows for a lower root-mean-square error ($2.1\,\mathrm{mm}$ on x axis, $2.5\,\mathrm{mm}$ on y axis) compared to the CTC ($3.4\,\mathrm{mm}$ on x axis, $3.8\,\mathrm{mm}$ on y axis). Moreover, the trajectory with the CTC is jerky (see associated video material https://youtu.be/6a4gE4A6bLU) with the

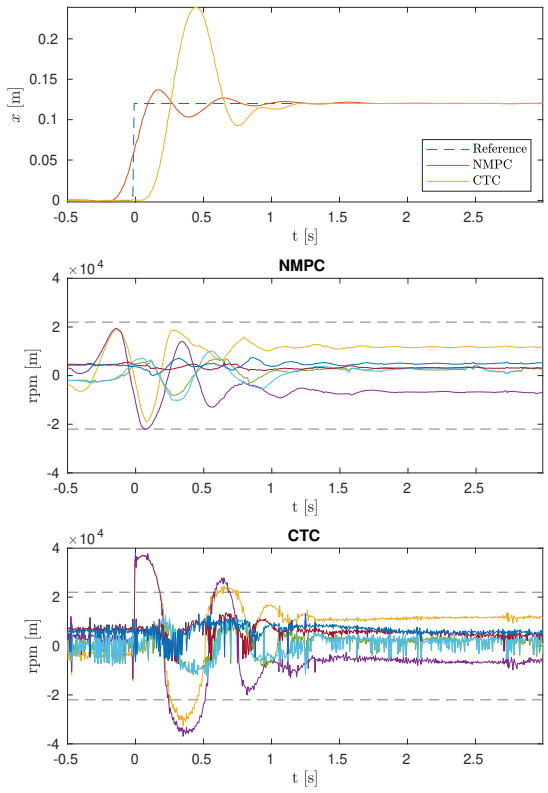

Fig. 5. Responses for a position step and control inputs (dashed lines are actuator saturation).

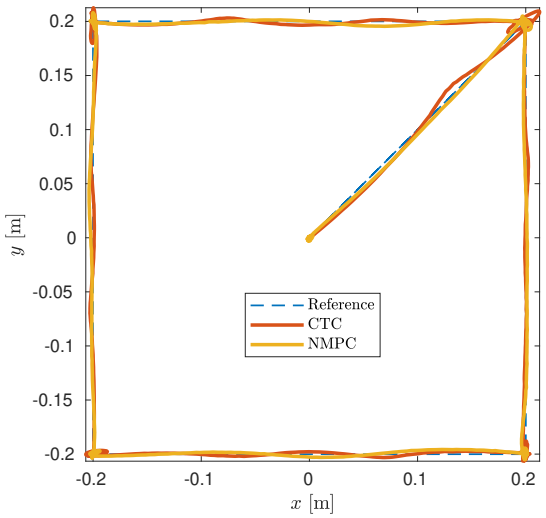

Fig. 6. Trajectory tracking by the AMES.

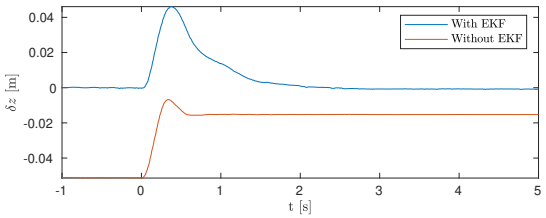

Fig. 7. NMPC disturbance rejection under load variation.

trapezoidal velocity profile used for each edge of the square. The feedforward path of the CTC is composed of the desired trajectory acceleration and thus is discontinuous. In contrast, the NMPC penalizes the rate of variation of the propeller velocity and ensures smoother behavior.

C. Disturbance rejection

In order to validate experimentally the ability of the NMPC to reject a constant disturbance, an $0.5\,\mathrm{kg}$ load is attached at the bottom of the AWG, corresponding to one fourth of its mass. Figure 7 shows the displacement δz along the z axis relatively to the equilibrium position ($\delta z = 0$) with and without the EKF disturbance estimator. Without the disturbance estimation, the AWG has a $50\,\mathrm{mm}$ steady-state error visible at $t < 0$ on the figure. When the load is cut off at $t = 0$, a $15\,\mathrm{mm}$ error persists. Adding the disturbance observer eliminates the steady-state error with a return of the AWG to its target position in less than $2\,\mathrm{s}$.

D. Energy efficiency

Since the NMPC objective function penalizes the energy of the control inputs, i.e. the rate of variation of the propeller velocity references, the motors are less prone to high accelerations. It results in a reduction of current draws and consequently power consumption. We compare the energy consumption of the AWG for the previous trajectory with the NMPC and the CTC in Fig. 8. For the same trajectory, the NMPC requires 1.4 times less energy.

VII. CONCLUSIONS AND FUTURE WORK

In this paper, we implement a NMPC to track a 6-DoF trajectory with an aerial manipulator with elastic suspension. The plant model is augmented with constant disturbances to eliminate steady-state errors. We test experimentally the NMPC and compare it to a CTC with an integral action.

We show that the NMPC improves the dynamic performance of the AMES compared to the CTC, but with a higher computational cost. The NMPC allows for a better handling of the saturations, a lower noise sensitivity, an improved trajectory tracking accuracy and a lower energy consumption.

The model accuracy can be improved by considering current saturations limiting the propeller speed of change.

The NMPC includes control allocation and so it is well adapted to deal with redundancies. Therefore, it is a good candidate for the simultaneous control of the AMES and its robotic carrier.

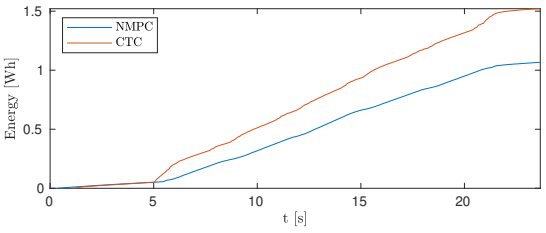

Fig. 8. Energy consumption of the AMES.

REFERENCES

[1] F. Ruggiero, V. Lippiello, and A. Ollero, "Aerial Manipulation: A Literature Review," *IEEE Robotics and Automation Letters*, vol. 3, no. 3, pp. 1957–1964, 7 2018. [Online]. Available: https://ieeexplore.ieee.org/document/8299552/

[2] M. Tognon and A. Franchi, "Omnidirectional Aerial Vehicles With Unidirectional Thrusters: Theory, Optimal Design, and Control," *IEEE Robotics and Automation Letters*, vol. 3, no. 3, pp. 2277–2282, 7 2018. [Online]. Available: http://ieeexplore.ieee.org/document/8281444/

[3] D. Brescianini and R. D'Andrea, "An omni-directional multirotor vehicle," *Mechatronics*, vol. 55, pp. 76–93, 11 2018. [Online]. Available: https://linkinghub.elsevier.com/retrieve/pii/S0957415818301314

[4] S. Park, J. Lee, J. Ahn, M. Kim, J. Her, G.-H. Yang, and D. Lee, "ODAR: Aerial Manipulation Platform Enabling Omnidirectional Wrench Generation," *IEEE/ASME Transactions on Mechatronics*, vol. 23, no. 4, pp. 1907–1918, 8 2018. [Online]. Available: https://ieeexplore.ieee.org/document/8401328/

[5] M. Brunner, K. Bodie, M. Kamel, M. Pantic, W. Zhang, J. Nieto, and R. Siegwart, "Trajectory Tracking Nonlinear Model Predictive Control for an Overactuated MAV," in *2020 IEEE International Conference on Robotics and Automation (ICRA)*. IEEE, 5 2020, pp. 5342–5348. [Online]. Available: https://ieeexplore.ieee.org/document/9197005/

[6] B. Houska, H. J. Ferreau, and M. Diehl, "ACADO toolkit-An open-source framework for automatic control and dynamic optimization," *Optimal Control Applications and Methods*, vol. 32, no. 3, pp. 298–312, 5 2011. [Online]. Available: http://doi.wiley.com/10.1002/oca.939

[7] D. Bicego, J. Mazzetto, R. Carli, M. Farina, and A. Franchi, "Nonlinear Model Predictive Control with Enhanced Actuator Model for Multi-Rotor Aerial Vehicles with Generic Designs," *Journal of Intelligent & Robotic Systems*, 9 2020. [Online]. Available: http://link.springer.com/10.1007/s10846-020-01250-9

[8] Y. Chen, M. Bruschetta, E. Picotti, and A. Beghi, "MATMPC - A MATLAB Based Toolbox for Real-time Nonlinear Model Predictive Control," in *2019 18th European Control Conference (ECC)*. IEEE, 6 2019, pp. 3365–3370. [Online]. Available: https://ieeexplore.ieee.org/document/8795788/

[9] M. Tognon and A. Franchi, *Theory and Applications for Control of Aerial Robots in Physical Interaction Through Tethers*, ser. Springer Tracts in Advanced Robotics. Cham: Springer International Publishing, 2021, vol. 140. [Online]. Available: http://link.springer.com/10.1007/978-3-030-48659-4

[10] Y. S. Sarkisov, M. J. Kim, D. Bicego, D. Tsetserukou, C. Ott, A. Franchi, and K. Kondak, "Development of SAM: cable-Suspended Aerial Manipulator *," in *2019 International Conference on Robotics and Automation (ICRA)*. IEEE, 5 2019, pp. 5323–5329. [Online]. Available: https://ieeexplore.ieee.org/document/8793592/

[11] Y. S. Sarkisov, M. Jun Kim, A. Coelho, D. Tsetserukou, C. Ott, and K. Kondak, "Optimal Oscillation Damping Control of cable-Suspended Aerial Manipulator with a Single IMU Sensor," in *2020 IEEE International Conference on Robotics and Automation (ICRA)*. IEEE, 5 2020, pp. 5349–5355. [Online]. Available: https://ieeexplore.ieee.org/document/9197055/

[12] A. Yiğit, G. Grappe, L. Cuvillon, S. Durand, and J. Gangloff, "Preliminary Study of an Aerial Manipulator with Elastic Suspension," in *2020 IEEE International Conference on Robotics and Automation (ICRA)*. IEEE, 5 2020, pp. 4287–4293. [Online]. Available: https://ieeexplore.ieee.org/document/9196942/

[13] R. Verschueren, G. Frison, D. Kouzoupis, N. van Duijkeren, A. Zanelli, B. Novoselnik, J. Frey, T. Albin, R. Quirynen, and M. Diehl, "acados: a modular open-source framework for fast embedded optimal control," 10 2019. [Online]. Available: http://arxiv.org/abs/1910.13753

[14] G. Frison and M. Diehl, "HPIPM: a high-performance quadratic programming framework for model predictive control," 3 2020. [Online]. Available: http://arxiv.org/abs/2003.02547

[15] H. Sellet, I. Khayour, L. Cuvillon, S. Durand, and J. Gangloff, "Active Damping of Parallel Robots Driven by Flexible Cables Using Cold-Gas Thrusters," in *2019 International Conference on Robotics and Automation (ICRA)*. IEEE, 5 2019, pp. 530–536. [Online]. Available: https://ieeexplore.ieee.org/document/8794061/

[16] I. Khayour, L. Cuvillon, C. Butin, A. Yiğit, S. Durand, and J. Gangloff, "Improving Disturbance Rejection and Dynamics of Cable Driven Parallel Robots with On-board Propellers," in *2020 IEEE/RSJ International Conference on Intelligent Robots and Systems (IROS)*. IEEE, 2020.

[17] W. Khan and M. Nahon, "Toward an Accurate Physics-Based UAV Thruster Model," *IEEE/ASME Transactions on Mechatronics*, vol. 18, no. 4, pp. 1269–1279, 8 2013. [Online]. Available: http://ieeexplore.ieee.org/document/6523983/

[18] G. Pannocchia, M. Gabiccini, and A. Artoni, "Offset-free MPC explained: novelties, subtleties, and applications," *IFAC-PapersOnLine*, vol. 48, no. 23, pp. 342–351, 2015. [Online]. Available: https://linkinghub.elsevier.com/retrieve/pii/S2405896315025884

[19] J. Gangloff, A. Yiğit, and M. Lesellier, "RPIt," 2020. [Online]. Available: https://github.com/jacqu/RPIt/

[20] B. Houska, H. J. Ferreau, and M. Diehl, "An auto-generated real-time iteration algorithm for nonlinear MPC in the microsecond range," *Automatica*, vol. 47, no. 10, pp. 2279–2285, 10 2011. [Online]. Available: https://linkinghub.elsevier.com/retrieve/pii/S0005109811003918